

# Analysis of the L3 BEC at $Z^0$ -pole

– Comparison of the conventional formula against the  $\tau$ -model –

Takuya Mizoguchi<sup>1</sup>, Seiji Matsumoto<sup>2</sup>, and Minoru Biyajima<sup>2</sup>

<sup>1</sup>National Institute of Technology, Toba College, Toba 517-8501, Japan

<sup>2</sup>Center for General Education, Shinshu University, Matsumoto 390-8621, Japan

## Abstract

The L3 Collaboration reported data on 2-jet and 3-jet Bose–Einstein correlations (BECs) with the results obtained through the  $\tau$ -model in 2011. In this study, we analyze these correlations using the conventional formula with the Gaussian long-range correlation ( $\text{CF} \times \text{LRC}_{(\text{Gauss})}$ ). The estimated ranges of interactions for 2-jet and 3-jet,  $R_{2\text{-jet}}$  and  $R_{3\text{-jet}}$ , have almost the same magnitude as those by  $\tau$ -model:  $R_{2\text{-jet}} = 0.83 \pm 0.05$  fm and  $R_{3\text{-jet}} = 1.09 \pm 0.04$  fm. The anticorrelation in BEC (less than 1.0) observed by the L3 Collaboration is related to the partially negative density profile ( $\rho_{\tau, \text{BE}}(\xi)$  in  $\xi$  space) in the  $\tau$ -model and the  $\text{LRC}_{(\text{Gauss})} = 1/(1 + \alpha e^{-\beta Q^2})$  in  $\text{CF}_1 \times \text{LRC}_{(\text{Gauss})}$ , respectively. Remarkably, the probability  $P_\tau(\xi)$  calculated from the Levy canonical form exhibits partially negative behavior.

## 1 Introduction

This study investigates the Bose–Einstein correlation (BEC) described by double ratios (DRs) in  $e^+e^-$  collisions at  $Z^0$ -pole [1] using the conventional formula [2, 3]. Because L3 Collaboration reported the separated data on 2-jet events and 3-jet events, we are very interested in.

DR is defined by single ratios, i.e.,  $C_2^{\text{data}}(Q) = N^{(2+:2-;Q)}/N^{(+;-;Q)}$  and  $C_2^{\text{MC}}(Q) = N_{\text{MC}}^{(2+:2-;Q)}/N_{\text{MC}}^{(+;-;Q)}$ , where  $N$  represents the number of events in the data and Monte Carlo events. The suffixes (2+ : 2-) and (+-) indicate charge combinations.  $Q = \sqrt{-(p_1 - p_2)^2}$  is the magnitude of the four-momentum transfer between two pions.

$$\begin{aligned} \text{DR} &= \frac{C_2^{\text{data}}(Q)}{C_2^{\text{MC}}(Q)} \\ &= \frac{N^{(2+:2-;Q)}/N^{(+;-;Q)}}{N_{\text{MC}}^{(2+:2-;Q)}/N_{\text{MC}}^{(+;-;Q)}} \end{aligned} \quad (1)$$

The L3 Collaboration analyzed the 2-jet and 3-jet data using the following  $\tau$ -model based on the Levy canonical form to explain the anticorrelation (BEC:less than 1.0) observed in the interval  $0.5 \text{ GeV} < Q < 1.5 \text{ GeV}$ :

$$F_\tau = [1 + \lambda \cos((R_a Q)^{\alpha_\tau}) \exp(-(RQ)^{\alpha_\tau})] \times \text{LRC}_{(\text{linear})}, \quad (2)$$

where  $R$  denotes the magnitude of the interaction region and  $R_a$  report a parameter expressed by  $R_a^{\alpha_\tau} = \tan(\alpha_\tau \pi/4) R^{\alpha_\tau}$ . The long-range correlation ( $\text{LRC}_{(\text{linear})}$ ) is the expression  $\text{LRC}_{(\text{linear})} = C(1 + \delta Q)$ , where  $\lambda$  denotes the degree of coherence, and  $\alpha_\tau$  represents the characteristic index introduced in the stochastic theory [4, 5].

Table 1 and Fig. 1 present the results estimated using Eq. (2). As seen in Table 1, the role of  $\text{LRC}_{(\text{linear})}$  is considerably important. In other words, the term of  $\cos((R_a Q)^{\alpha_\tau})$  cannot sufficiently explain the anticorrelation. To know the role of  $R_a^{\alpha_\tau} = \tan(\alpha_\tau \pi/4) R^{\alpha_\tau}$ , we present our analysis without the constraint  $R_a^{\alpha_\tau}$ , i.e., through an adjustable parameter mentioned in Appendix A.

Table 1: Fit parameters of data on 2-jet and 3-jet events by Eq. (2).  $R_a^{\alpha\tau} = \tan(\alpha\tau\pi/4)R^{\alpha\tau}$  is calculated in the exact form. In the upper column,  $\delta = 0$  is used.

event	$R$ (fm)	$\lambda$	$C$	$\alpha_\tau$	$\delta$ ( $\text{GeV}^{-1}$ )	$\chi^2/\text{dof}$
2-jet	$0.75 \pm 0.03$	$0.58 \pm 0.02$	$0.986 \pm 0.001$	$0.91 \pm 0.02$	—	119.7/96
3-jet	$0.93 \pm 0.03$	$0.78 \pm 0.03$	$0.989 \pm 0.001$	$0.87 \pm 0.01$	—	226.8/96
2-jet	$0.78 \pm 0.04$	$0.61 \pm 0.03$	$0.979 \pm 0.002$	$0.88 \pm 0.02$	$(4.6 \pm 0.9) \times 10^{-3}$	94.6/95
3-jet	$0.99 \pm 0.04$	$0.85 \pm 0.04$	$0.977 \pm 0.001$	$0.83 \pm 0.01$	$(7.7 \pm 0.7) \times 10^{-3}$	113/95

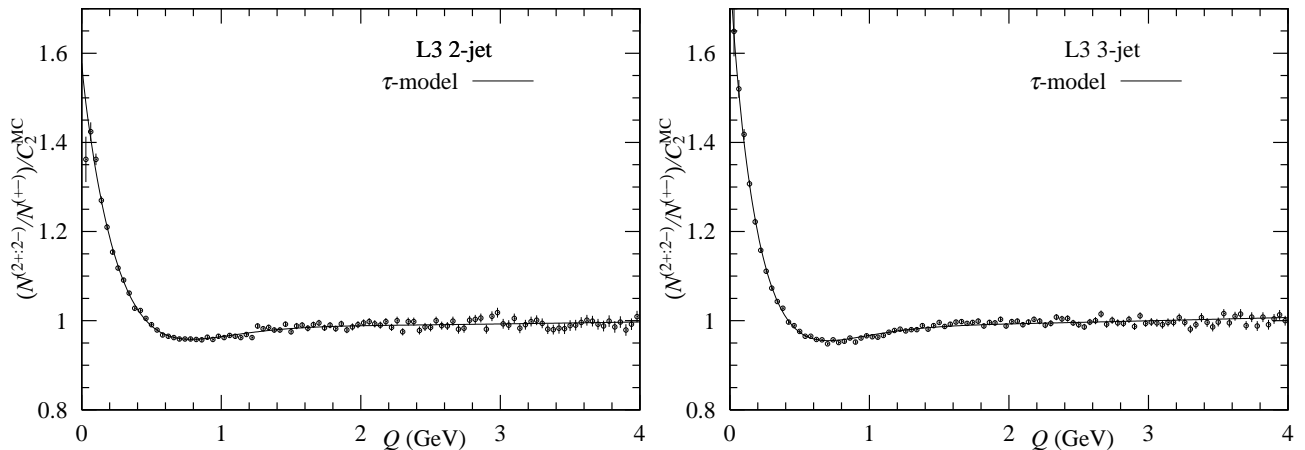


Figure 1: Analysis of data by Eq. (2).

This paper aims to analyze the 2-jet and 3-jet BECs using the conventional formula  $\text{CF}_I$  with  $\text{LRC}_{(\text{Gauss})}$  which are expressed as follows:

$$\text{CF}_I = 1 + \lambda E_{\text{BE}}, \quad (3)$$

$$\text{and } \text{LRC}_{(\text{Gauss})} = \frac{C}{1 + \alpha \exp(-\beta Q^2)}. \quad (4)$$

where  $E_{\text{BE}}$  is the exchange function due to Bose–Einstein statistics.  $\text{LRC}_{(\text{Gauss})}$  was derived by us in Ref. [3] via analysis of CMS Monte Carlo events at 13 TeV in LHC reported in Ref. [4]. On the contrary, it should be noted that L3 Collaboration did not report their MC data. Thus we assume Eq. (4) in the present study.

We consider the following four functions based on our previous study [6]:

$$E_{\text{BE}} = \exp(-(RQ)^2) \text{ (Gaussian distribution)}, \quad (5)$$

$$E_{\text{BE}} = \exp(-RQ) \text{ (Exponential function)}, \quad (6)$$

$$\text{and } E_{\text{BE}} = \frac{1}{(1 + (RQ)^2)^s} \text{ (Inverse power law: } s = 2 \text{ and } s = 5/2). \quad (7)$$

The remainder of this paper is organized as follows. In Section 2, we analyze the data for 2-jet and 3-jet using Eqs. (3)~(7). In Section 3, we study the profiles of the exchange function  $E$  of 2-jet and 3-jet in  $\xi$ -space, where  $\xi = \sqrt{(x_1 - x_2)^2 + (y_1 - y_2)^2 + (z_1 - z_2)^2 + (ct_1 - ct_2)^2}$ . Finally, Section 4 presents the concluding remarks.

In Appendix A, we present the results obtained using Eq. (2), but the constraint  $R_a$ 's are treated as the adjustable parameters; this indicates that the constraint is free. In Appendix B, data on  $N_{\text{MC}}^{(2+:2-)} / N_{\text{MC}}^{(+-)}$  at  $Z^0$ -pole by DELPHI Collaboration is presented. In Appendix C, the Levy canonical form and several formulations calculated using the inverse Fourier transformation are presented.

## 2 Analysis of data on 2-jet and 3-jet using $CF_I$ with $LRC_{(\text{linear})}$ and $LRC_{(\text{Gauss})}$

### I: Application of Eq. (3) with Eqs. (4)~(6)

Using Eqs. (4), (5), and (6), we analyzed the 2-jet and 3-jet with  $LRC_{(\text{linear})}$  and  $LRC_{(\text{Gauss})}$ . Our results are presented in Table 2.

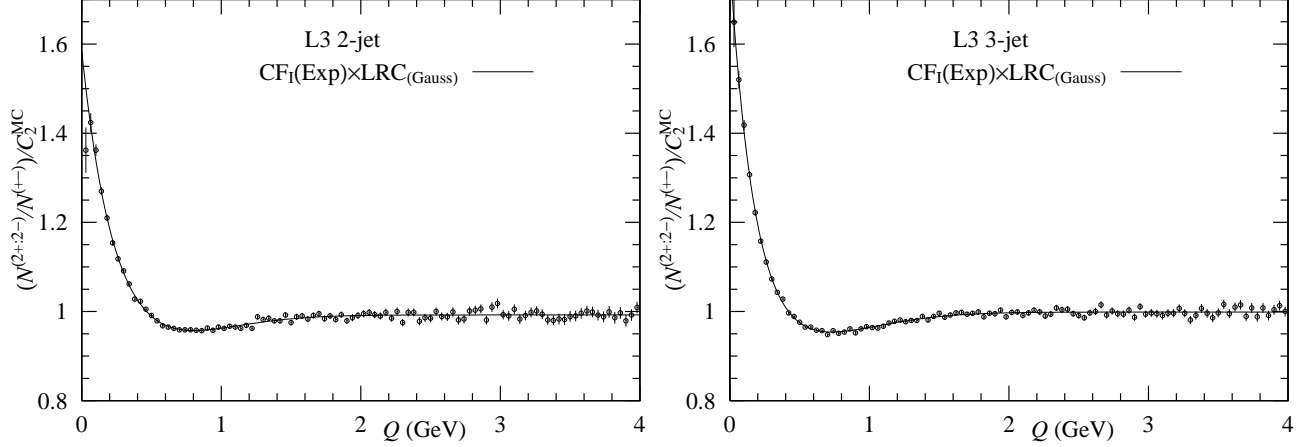


Figure 2: Analysis of data using Eqs. (3), (4), and (6)

Table 2: Fit parameters of data on 2-jet and 3-jet events using  $CF_I$  with  $LRC_{(\text{linear})}$  and  $LRC_{(\text{Gauss})}$

$LRC_{(\text{linear})}$		$\lambda$	$C$	$\delta$ ( $\text{GeV}^{-1}$ )	$\chi^2/\text{dof}$	
$E_{BE}$	$R$ (fm)					
2-jet						
G	$0.68 \pm 0.01$	$0.41 \pm 0.01$	$0.956 \pm 0.002$	$(1.34 \pm 0.09) \times 10^{-2}$	247/96	
E	$1.18 \pm 0.02$	$0.80 \pm 0.02$	$0.947 \pm 0.002$	$(1.75 \pm 0.10) \times 10^{-2}$	255/96	
IP2.0	$0.64 \pm 0.01$	$0.52 \pm 0.01$	$0.946 \pm 0.002$	$(1.79 \pm 0.10) \times 10^{-2}$	247/96	
IP2.5	$0.54 \pm 0.01$	$0.49 \pm 0.01$	$0.949 \pm 0.002$	$(1.67 \pm 0.10) \times 10^{-2}$	231/96	
3-jet						
G	$0.79 \pm 0.01$	$0.51 \pm 0.01$	$0.953 \pm 0.001$	$(1.74 \pm 0.07) \times 10^{-2}$	455/96	
E	$1.44 \pm 0.02$	$1.06 \pm 0.02$	$0.945 \pm 0.001$	$(2.10 \pm 0.08) \times 10^{-2}$	438/96	
IP2.0	$0.77 \pm 0.01$	$0.68 \pm 0.01$	$0.943 \pm 0.001$	$(2.19 \pm 0.08) \times 10^{-2}$	472/96	
IP2.5	$0.65 \pm 0.01$	$0.64 \pm 0.01$	$0.946 \pm 0.001$	$(2.07 \pm 0.08) \times 10^{-2}$	436/96	
$LRC_{(\text{Gauss})}$		$\lambda$	$C$	$\alpha$	$\beta$ ( $\text{GeV}^{-2}$ )	$\chi^2/\text{dof}$
$E_{BE}$	$R$ (fm)					
2-jet						
G	$0.65 \pm 0.01$	$0.40 \pm 0.01$	$0.995 \pm 0.002$	$0.046 \pm 0.003$	$0.49 \pm 0.07$	199/95
E	$0.83 \pm 0.05$	$0.82 \pm 0.03$	$0.992 \pm 0.001$	$0.137 \pm 0.024$	$1.15 \pm 0.12$	90.0/95
IP2	$0.55 \pm 0.01$	$0.52 \pm 0.01$	$0.993 \pm 0.001$	$0.802 \pm 0.006$	$0.77 \pm 0.08$	118/95
IP2.5	$0.48 \pm 0.01$	$0.49 \pm 0.01$	$0.994 \pm 0.002$	$0.701 \pm 0.005$	$0.725 \pm 0.08$	126/95
3-jet						
G	$0.75 \pm 0.01$	$0.50 \pm 0.01$	$1.001 \pm 0.001$	$0.058 \pm 0.002$	$0.57 \pm 0.05$	310/95
E	$1.09 \pm 0.04$	$0.99 \pm 0.02$	$0.999 \pm 0.001$	$0.115 \pm 0.009$	$1.06 \pm 0.08$	83.9/95
IP2.0	$0.65 \pm 0.01$	$0.65 \pm 0.01$	$1.000 \pm 0.001$	$0.093 \pm 0.004$	$0.84 \pm 0.06$	140/95
IP2.5	$0.56 \pm 0.01$	$0.62 \pm 0.01$	$1.000 \pm 0.001$	$0.083 \pm 0.004$	$0.79 \pm 0.06$	157/95

As shown in Tables 1 and 2, our results from Eq. (6) and  $LRC_{(\text{Gauss})}$  are compatible with those

presented in Table 1. However, the degree of coherence  $\lambda$ 's presented in Table 1 are somewhat smaller than those presented in Table 2. In Appendix A, we present our results for no constraints.

## II: Analysis of 2-jet and 3-jet events using the quantum optics approach

As shown in Table 2, the degree of coherence  $\lambda = 0.82 \pm 0.03$  in  $\text{CF}_I(\text{exp}) \times \text{LRC}_{(\text{Gauss})}$  is observed. To consider its meaning, we use the following formula with quantum optics (QO) [7, 8].

$$F_{\text{QO}} = (1 + p^2 e^{-RQ} + 2p(1-p)e^{-RQ/2}) \times \text{LRC}_{(\text{Gauss})}, \quad (8)$$

where  $p = A/\langle n \rangle_{\text{tot}}$  represents the ratio of the chaotic component to the total multiplicity.  $1 - p = \langle n \rangle_{\text{coherent}}/\langle n \rangle_{\text{tot}}$  denotes the ratio of the coherent component to the total one. For the 2-jet event, as shown in Table 3,  $1 - p \cong 0.3$ , the coherent component is approximately 30%. Moreover,  $R \cong 1.06 \pm 0.10$  fm is larger than those in Table 2. This is attributed to the third term  $2p(1-p)e^{-RQ/2}$ .

Table 3: Fit parameters of data on 2-jet and 3-jet events using Eq. (7)

event	$R$ (fm)	$p$	$C$	$\alpha$	$\beta$ ( $\text{GeV}^{-2}$ )	$\chi^2/\text{dof}$
2-jet	$1.06 \pm 0.10$	$0.71 \pm 0.04$	$0.992 \pm 0.001$	$0.19 \pm 0.02$	$1.12 \pm 0.05$	90.4/95
3-jet	$1.11 \pm 0.04$	$0.98 \pm 0.02$	$0.999 \pm 0.001$	$0.12 \pm 0.01$	$1.07 \pm 0.07$	83.6/95

For the 3-jet event, in Eq. (8), we obtain  $p = 0.98 \pm 0.02$ , meaning that  $p = A/\langle n \rangle_{\text{tot}} \cong 1.0$ . There is no contribution from the coherent component, because  $1 - p \cong 0.0$ . We conclude that the data on the 3-jet events are almost chaotic [9]. See also Ref. [10] for comparison.

## 3 Mechanism of anticorrelation and profiles of the source functions of 2-jet and 3-jet BECs in the $\xi$ -space

### I: Explanation of the anticorrelation

The anticorrelation in the 2-jet and 3-jet is observed in the region  $0.5 \leq Q \leq 1.5$  GeV. These values in BEC are smaller than 1.0. These behaviors can be explained in two ways.

In the conventional formula with the function,  $\text{CF}_I(\text{Exp}) \times \text{LRC}_{(\text{Gauss})}$ , the anticorrelation is explained by the Gaussian function with  $\text{LRC}_{(\text{Gauss})} - 1 = \sum_{k=1}^{\infty} (-\alpha)^k \exp(-k\beta Q^2)$ . Second, the cross term which is a product of the exponential function and  $(\text{LRC}_{(\text{Gauss})} - 1)$ :  $F_{\text{cross}}(Q) = e^{-RQ} \sum_{k=1}^{\infty} (-\alpha)^k e^{-k\beta Q^2}$ . For reference, we present data on  $N_{\text{MC}}^{(2+:2-)} / N_{\text{MC}}^{(+-)}$  at  $Z^0$ -ploe by DELPHI Collaboration [14] in Appendix B because we have no information on them by L3 Collaboration at present.

Furthermore, in the  $\tau$ -model, the anticorrelation is described by the cosine  $[(R_a Q)^{\alpha\tau}]$  in the exchange function. Indeed, this mechanism is shown in Fig. 3. The behavior of  $\cos((R_a Q)^{\alpha\tau})$  is oscillating. By multiplying  $\exp(-(RQ)^{\alpha\tau})$ , the anticorrelation is created.

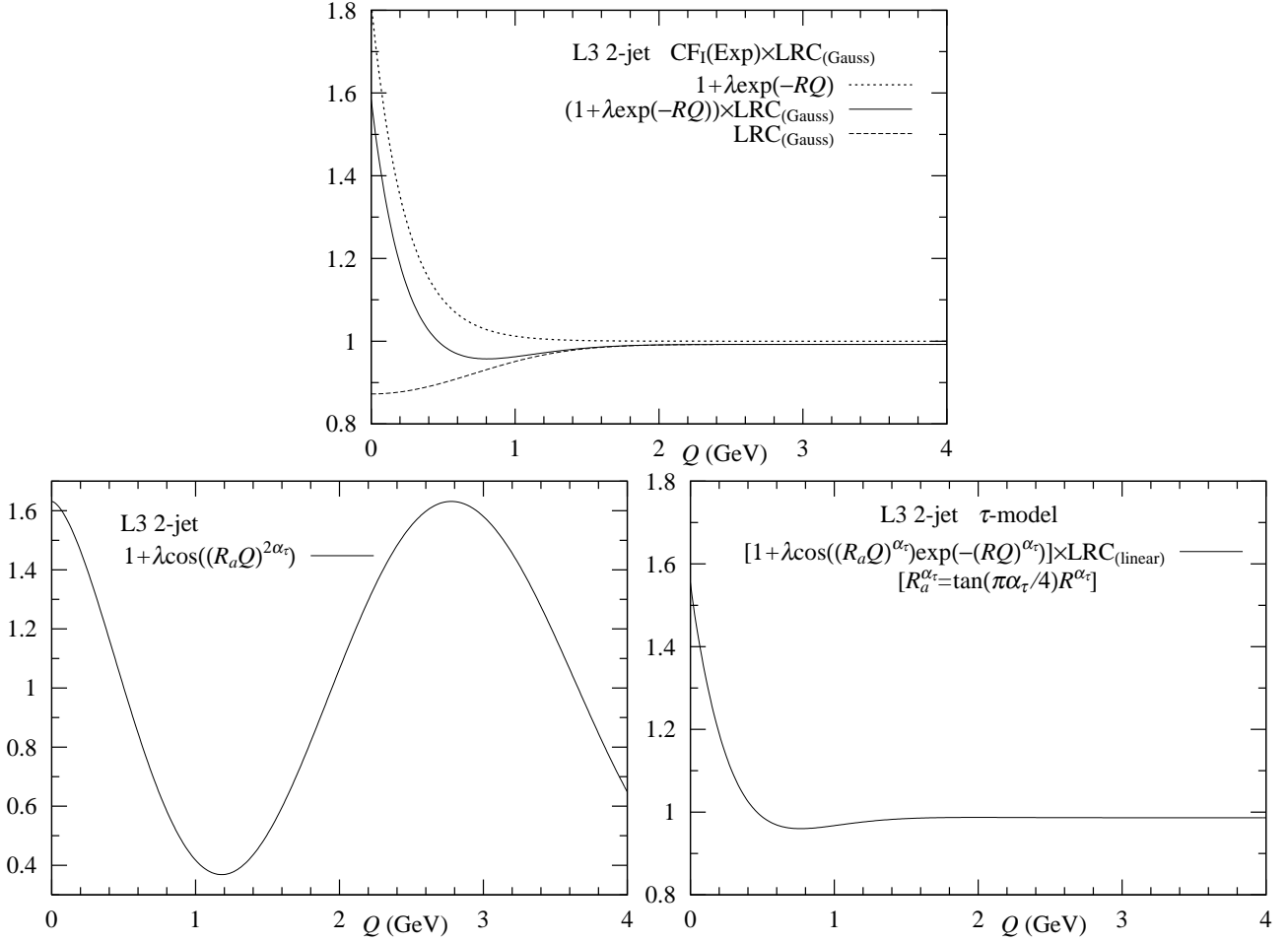


Figure 3: Mechanism of “anticorrelation” in  $CF_I \times LRC_{(\text{Gauss})}$  and the  $\tau$ -model.

## II: Source functions of BEC in the $\xi$ -space

Using the Fourier transform of  $E_{\text{BE}}$ 's and  $LRC_{(\text{Gauss})}$ , we calculate the profiles of  $CF_I \times LRC_{(\text{Gauss})}$  and the  $\tau$ -model in the  $\xi$ -space, which are expressed as the density  $\rho(\xi)$ s.

We use the following expansion to study the profile of  $CF_I \times LRC_{(\text{Gauss})}$  in the  $\xi$ -space. Before concrete computation, we add the physical meaning.  $\rho_{\text{Exp}}(\xi)$  is interpreted as  $N = 4$  dimensional Lorentz distribution because  $(N + 1)/2 = (4 + 1)/2 = 5/2$  (see Ref. [11]).  $\rho_{\text{Gauss}}(\xi)$  is connected to  $\exp(-\beta Q^2)$  in the  $LRC_{(\text{Gauss})}$ .

$$\begin{cases} \rho_{\text{Exp}}(\xi) = \frac{3}{4\pi^2 R^4} \frac{1}{(1 + (\xi/R)^2)^{5/2}}, \\ S_{\text{BE}}(\xi) = 2\pi^2 \xi^3 \rho_{\text{Exp}}(\xi). \end{cases} \quad (9)$$

The source function of the  $LRC_{(\text{Gauss})}$  is calculated as follows:

$$\begin{cases} \rho_{\text{Gauss}}(\xi) = \frac{1}{16\pi^2 R^4} \exp\left(-\frac{\xi^2}{4R^2}\right), \\ S_{\text{BG}}(\xi) = 2\pi^2 \xi^3 \sum_{k=1}^{\infty} (-\alpha)^k \rho_{\text{Gauss}}(\xi, R = \sqrt{k\beta}). \end{cases} \quad (10)$$

The contribution from the cross term,  $e^{-RQ} \times LRC_{(\text{Gauss})}$ , is computed by the inverse Fourier transformation ( $N = 4$ ) and the numerical integration.

For the stochastic density of the exchange function  $E_{\text{BE}}$  in the  $\tau$ -model, we first employ the following numerical calculation:

$$\begin{cases} E_{\text{BE}}^{(\tau)} = \exp(-aQ^{\alpha_\tau}) \cos(bQ^{\alpha_\tau}), \\ \rho_{\tau,\text{BE}}(\xi) = \frac{1}{(2\pi)^2 \xi} \int_0^\infty Q^2 E_{\text{BE}}^{(\tau)} J_1(Q\xi) dQ \end{cases} \quad (11)$$

where  $J_1(Q\xi)$  is the Bessel function [6]. Fig. 4 shows the numerical calculation of Eq. (11).

Second, we derive the analytic expression (i.e., the series expansion) of Eq. (11) based on Refs. [11,12]:

$$\begin{aligned} & \text{Series expansion of } \rho_{\tau,\text{BE}}(\xi) \\ &= \frac{1}{(2\pi)^2 \xi} \frac{1}{\alpha_\tau} \sum_{k=0}^{\infty} \left(\frac{\xi}{2}\right)^{2k+1} \frac{(-1)^k \Gamma\left(\frac{4+2k}{\alpha_\tau}\right)}{\Gamma(k+1)\Gamma(k+2)} \frac{1}{(a^2 + b^2)^{(4+2k)/(2\alpha_\tau)}} \cos\left(\frac{4+2k}{\alpha_\tau} \arctan\left(\frac{b}{a}\right)\right) \end{aligned} \quad (12)$$

Table 4: Typical numerical coefficients in Eq. (12) for the 2-jet event. See Table 1.

$k$	$\frac{1}{(a^2 + b^2)^{(4+2k)/(2\alpha_\tau)}$	$\cos\left(\frac{4+2k}{\alpha_\tau} \arctan\left(\frac{b}{a}\right)\right)$
0	0.600	-0.903
1	0.464	0.617
2	0.359	0.632
3	0.278	-0.895

As shown in Table 4 and Fig. 4, the partially negative behavior of the density profile ( $0 \leq \xi \leq 0.5$  fm) arises from the first term of  $\cos\left(\frac{4+2k}{\alpha_\tau} \arctan\left(\frac{b}{a}\right)\right)\Big|_{k=0} \cong -0.903$  (See Table 1:  $a = 0.8293$ ,  $b = 0.7366$ , and  $\alpha_\tau = 0.8104$  are used [1]).

Table 5: Comparison of numerical computation of Eq. (11) and the series expansion of Eq. (12) using  $a = 0.8293$ ,  $b = 0.7366$ , and  $\alpha_\tau = 0.8104$ .

$\xi$ (fm)	numerical	series expansion	
	computation	$k_{\text{max}} = 20$	$k_{\text{max}} = 50$
0.01	$-3.642532 \times 10^{-6}$	$-3.642532 \times 10^{-6}$	$-3.642532 \times 10^{-6}$
0.05	$-4.603769 \times 10^{-4}$	$-4.603769 \times 10^{-4}$	$-4.603769 \times 10^{-4}$
0.10	$-3.801454 \times 10^{-3}$	$-3.801454 \times 10^{-3}$	$-3.801454 \times 10^{-3}$
0.15	$-1.339117 \times 10^{-2}$	$-1.339117 \times 10^{-2}$	$-1.339117 \times 10^{-2}$
0.20	$-3.299086 \times 10^{-2}$	$-3.299086 \times 10^{-2}$	$-3.299086 \times 10^{-2}$
0.25	$-6.527692 \times 10^{-2}$	$-6.527692 \times 10^{-2}$	$-6.527692 \times 10^{-2}$
0.30	$-1.086730 \times 10^{-1}$	$-1.086753 \times 10^{-1}$	$-1.086729 \times 10^{-1}$
0.31	$-1.180534 \times 10^{-1}$	$-1.180631 \times 10^{-1}$	$-1.180492 \times 10^{-1}$
0.32	$-1.274482 \times 10^{-1}$	$-1.274869 \times 10^{-1}$	$-1.273354 \times 10^{-1}$

Note:  $\xi = 0.3$  fm is the applicable limit of the series expansion. This limit is related to the asymptotic form of the Bessel function.

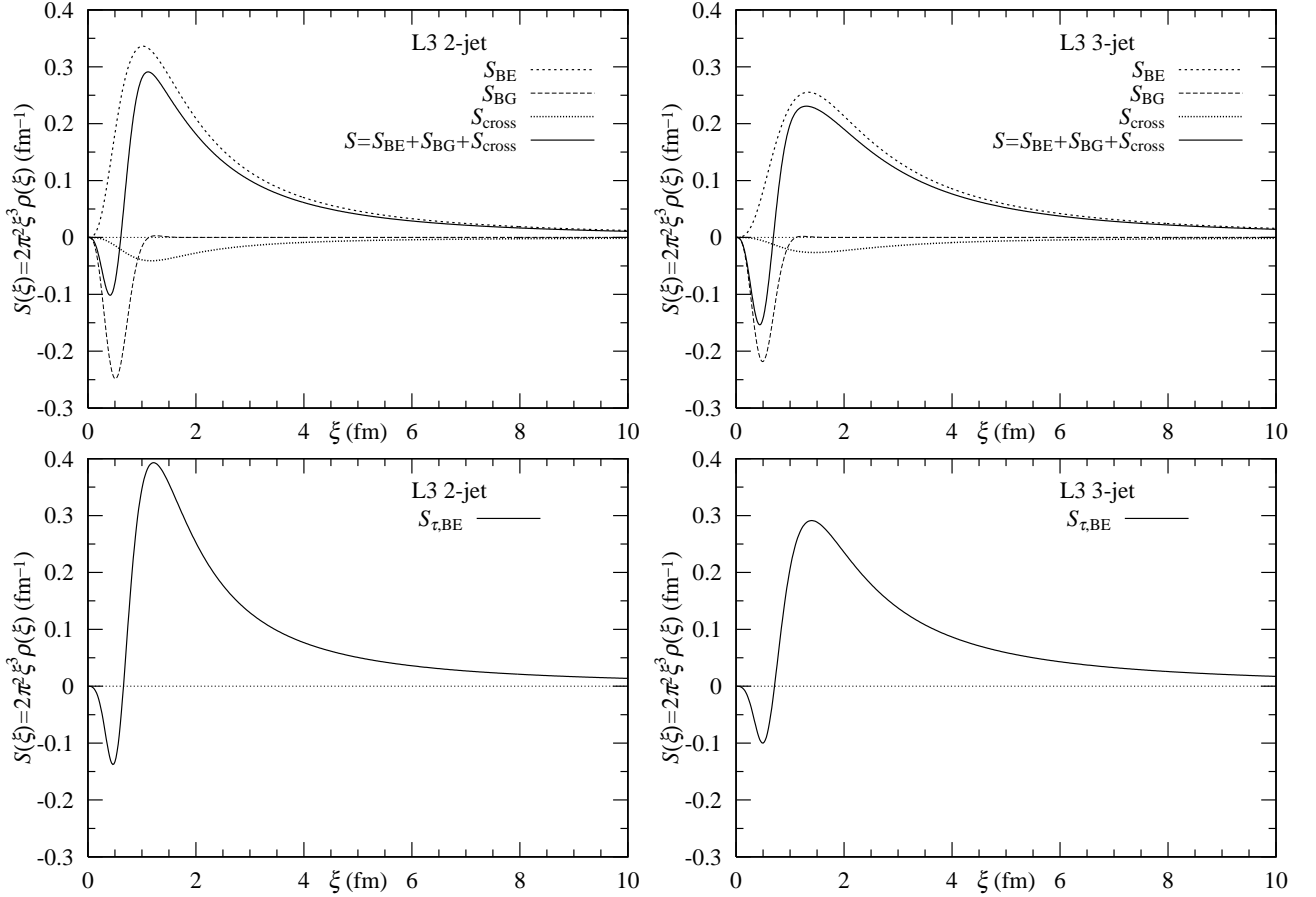


Figure 4: Source functions of  $CF_I(\text{Exp}) \times LRC_{(\text{Gauss})}$  and the  $\tau$ -model in  $\xi$ -space. The source functions of  $(LRC_{(\text{Gauss})} - 1)$  expressed by  $S_{BG}(\xi)$  are added in the upper figures. As  $R$  increases, the height of the peak decreases in the  $\tau$ -model. Estimated values in Tables 1 and 2 are used.

Fig. 4 shows the two types of behaviors for the 2-jet and 3-jet events. The dip structures at  $\xi \sim 0.5$  fm are observed. The dip structures in the 3-jet (right) are deeper than those in the 2-jet (left) in  $CF_I(\text{Exp}) \times LRC_{(\text{Gauss})}$ .

It can be said that, the negative profile of the density  $\rho(\xi)$  in  $CF_I \times LRC_{(\text{Gauss})}$  originates from the denominator of DR. In other words, the Monte Carlo calculation in the denominator of the DR in L3 BEC at  $Z^0$ -pole implies the clustering effect expressed by the Gaussian distribution as well as in the  $N_{MC}^{(2+;2-)}$  [3, 4].

In conclusion, we show comparison of results in  $\xi$  space by our approach and the  $\tau$ -model in Table 6. They are worthwhile to name of the pion femtoscopy.

Table 6: Comparison of physical pictures of our approach ( $\text{CF}_I(\text{Exp}) \times \text{LRC}_{(\text{Gauss})}$ ) and the  $\tau$ -model. In the  $\tau$ -model, the SRs  $N_{\text{data}}^{(2+;2-)} / N_{\text{data}}^{(+-)}$  and  $N_{\text{MC}}^{(2+;2-)} / N_{\text{MC}}^{(+-)}$  are not separated.

	$\xi$ -space	Momentum ( $Q$ )-space
Our approach ( $\text{CF}_I(\text{Exp})$ ) $\times \text{LRC}_{(\text{Gauss})}$	<p>The numerator:</p> $\rho_{\text{Lorentz}}(\xi, N = 4) = \frac{3}{4\pi^2 R^4} \frac{1}{(1 + (\xi/R)^2)^{5/2}}$ <p>where <math>5/2 = (N + 1)/2</math>. <math>N = 4</math> means 4-dimension.</p> <p>The denominator of LRC:</p> $\rho_{\text{Gauss}}(\xi, N = 4) = \frac{1}{16\pi^2 R^4} \exp\left(-\frac{\xi^2}{4R^2}\right).$ <p>See Ref. [6].</p>	$E_{\text{BE}} = e^{-RQ}.$  $\text{LRC} = \frac{C}{1 + \alpha \exp(-\beta Q^2)}$ $= C \sum_{k=0}^{\infty} (-\alpha)^k e^{-k\beta Q^2}.$ <p>which is reflecting the clustering effect observed in <math>N_{\text{MC}}^{(2+;2-)}</math> [3, 4]. See Ref. [14].</p>
$\tau$ -model	<p>The probability density and source function are calculated from <math>\tilde{H}_4(\omega)</math> in the right column.</p> $\rho_{\tau, \text{BE}}(\xi, \alpha_\tau) = \frac{1}{(2\pi)^2 \xi} \int_0^\infty Q^2 \exp(-aQ^{2\alpha_\tau}) \cdot \cos(bQ^{2\alpha_\tau}) J_1(Q\xi) dQ$ $S_{\tau, \text{BE}}(\xi) = 2\pi^2 \xi^3 \rho_{\tau, \text{BE}}(\xi, \alpha_\tau)$	<p>Levy canonical form (<math>\zeta = \tan(\alpha_\tau \pi/2)</math>)</p> $\tilde{H}_4(RQ) = \exp\left[-\frac{1}{2}(RQ)^{2\alpha}(1 - i\zeta)\right],$ $E_{\text{BE}} = \text{Re}\left[\tilde{H}_4^2(RQ)\right]$ $= \exp\left(-\frac{1}{2}(RQ)^{2\alpha}\right) \cos\left(\frac{1}{2}(RQ)^{2\alpha}\zeta\right).$ <p>See Appendix C. <math>\text{LRC} = C(1 + \delta Q)</math>.</p>

cf. The probability of the Levy canonical form ( $N = 1$  dimension) is expressed as

$$P(x; \alpha_\tau, \theta) = \frac{1}{\pi} \text{Re} \left[ \int_0^\infty dz \exp\left(-ixz - z^{\alpha_\tau} e^{i\frac{\pi}{2}\theta}\right) \right],$$

where  $\text{Re}[\ ]$  means the real part. The Lorentz (or Cauchy) distribution is obtained by

$P(x; 1, 0) = 1/[\pi(1 + x^2)]$ . The Gaussian one is obtained by  $P(x; 2, 0) = (1/\pi)e^{-x^2}$ . The formulas with  $N = 4$  are calculated by the following replacement in  $P(x; \alpha_\tau, \theta)$  above:  $ixz \rightarrow ixz \cos \phi$  and  $dz \rightarrow d^4z = \sin^2 \phi d\phi \cdot 4\pi z^2 dz$ .  $P_4(x; 1, 0) = 1/[\pi(1 + x^2)^{5/2}]$  and  $P_4(x; 2, 0) = \pi e^{-x^2/4}$  are obtained.

Concerning the Levy canonical form and the inverse Fourier transformation ( $N = 1$  and  $N = 4$ ), several formulations are shown in Appendix C.

## 4 Concluding remarks

**C1)** From our analysis of L3 BEC by  $\text{CF}_I(\text{Exp}) \times \text{LRC}_{(\text{Gauss})}$ , we have known that the anticorrelation (observed in 0.5 GeV  $Q < 1.5$  GeV) is related to the denominator of the DR. In the  $\text{CF}_I(\text{Exp}) \times \text{LRC}_{(\text{Gauss})}$ ,  $E_{\text{BE}} = \exp(-RQ)$  cooperates with  $\text{LRC}_{(\text{Gauss})}$  (see Fig. 4). Provided that the MC events at  $Z^0$ -pole by L3 Collaboration were reported, we are able to know whether or not the statement mentioned above is correct.

**C2)** On the other hand, in the  $\tau$ -model, the anticorrelation is explained by the imaginary part in the Levy canonical form. Indeed, through the analytic form of the exchange function  $\exp(-aQ^{2\alpha}) \cos(bQ^{2\alpha})$  in the  $\xi$ -space, we understand that the anticorrelation in BEC is related to the negative behavior therein.

**C3)** In the  $\tau$ -model, we obtain the analytic formula, i.e., the series expansion of  $\rho_{\tau, \text{BE}}(\xi)$  (see Eq. (12)). We can understand the negative behavior ( $\xi < 0.7$  fm) in the Levy canonical form in Fig. 4.

**C4)** Two estimated values  $R = 0.83 \pm 0.05$  fm (2-jet) and  $R = 1.09 \pm 0.04$  fm (3-jet) by  $\text{CF}_I(\text{Exp}) \times \text{LRC}_{(\text{Gauss})}$  (see Table 7) are compared with  $R = 0.78 \pm 0.04$  fm (2-jet) and  $R = 0.99 \pm 0.04$  fm (3-jet) estimated by  $\tau$ -model. Concerning 2-jet,  $R$ 's are coincide with each other. Furthermore, regarding 3-jet, they show different figures, as  $R_a$  is exact. When  $R_a$  is treated as the adjustable parameter, they are almost coincide because  $R = 1.07 \pm 0.05$  fm (3-jet) by  $\tau$ -model.

**C5)** We observe that the 3-jet BEC exhibits almost chaotic properties, provided that the theory of QO is applied. This indicates that it is an ideal event for the study of BEC. The phases of proceeded pions are completely randomized.

**D1)** To examine Eqs. (3) and (4) furthermore, we reinvestigate the role of the  $\text{LRC}_{(\text{Gauss})}$ . Therefore, we adopt the following exchange function [13]

$$E_{\text{BE}(\cos)} = e^{-RQ} \cos(R_p Q) \quad (13)$$

where  $R$  and  $R_p$  denote different interaction regions. Thus, we assume the following formula:

$$\text{CF}_I(\text{Exp} \cdot \cos) \times \text{LRC}_{(\text{Gauss})} = (1 + \lambda e^{-RQ} \cos(R_p Q)) \frac{C}{1 + \alpha \exp(-\beta Q^2)}. \quad (14)$$

Our results are shown in Table 7.

Table 7: Fit parameters of data on 2-jet and 3-jet events using Eq. (14)

event	$R$ (fm)	$R_p$ (fm)	$\lambda$	$C$	$\alpha$	$\beta$ (GeV <sup>-2</sup> )	$\chi^2/\text{dof}$
2-jet	$0.83 \pm 0.05$	$2.3 \times 10^{-4} \pm 0.87$	$0.82 \pm 0.03$	$0.992 \pm 0.001$	$0.137 \pm 0.026$	$1.15 \pm 0.12$	90.0/94
3-jet	$1.09 \pm 0.04$	$2.0 \times 10^{-5} \pm 0.17$	$0.99 \pm 0.02$	$0.999 \pm 0.001$	$0.115 \pm 0.009$	$1.06 \pm 0.08$	83.9/94

As shown in Table 7, the contribution from  $\cos(R_p Q)$  is almost one, indicating that the exponential function is suitable for the L3 BEC data.

**D2)** To examine whether or not  $\text{LRC}_{(\text{Gauss})}$  is profitable for  $\text{CF}_I(\text{Exp})$ , we assume the following expression:

$$\text{CF}_I(\text{Exp}) \times \text{LRC}_{(\text{fraction})} = (1 + \lambda e^{-RQ}) \frac{C}{1 + \alpha \exp(-\beta Q^\gamma)}. \quad (15)$$

where  $\gamma$  is a fractal number. Our results are shown in Table 8.

Table 8: Fit parameters of data on 2-jet and 3-jet events using Eq. (15)

event	$R$ (fm)	$\lambda$	$C$	$\alpha$	$\beta$ (GeV <sup>-<math>\gamma</math>)</sup>	$\gamma$	$\chi^2/\text{dof}$
2-jet	$0.86 \pm 0.12$	$0.79 \pm 0.10$	$0.992 \pm 0.002$	$0.12 \pm 0.08$	$1.03 \pm 0.48$	$2.19 \pm 0.82$	89.9/94
3-jet	$1.18 \pm 0.05$	$0.95 \pm 0.02$	$0.998 \pm 0.001$	$0.08 \pm 0.01$	$0.70 \pm 0.14$	$2.97 \pm 0.52$	80.2/94

As shown in Table 8, the result of the 2-jet event supports our framework. In contrast, the result of the 3-jet event suggests the  $\gamma = 3.0$ . These figures are compared with the Monte-Carlo calculation. Thus, we are expecting information on  $N_{\text{MC}}^{(2+;2-)}$  and  $N_{\text{MC}}^{(+-)}$  at  $Z^0$ -pole by L3 Collaboration.

**D3)** We are expecting a report on all-jet events by L3 Collaboration, because they contain the 2-jet and 3-jet events. In that case, the following formula of  $\text{CF}_{\text{II}}(\text{Exp}_1 + \text{Exp}_2) \times \text{LRC}_{(\text{Gauss})}$  could be applied:

$$(1 + \lambda_2 e^{-R_2 Q} + \lambda_3 e^{-R_3 Q}) \times \frac{C}{1 + \alpha \exp(-\beta Q^2)}, \quad (16)$$

where  $\lambda_2$ ,  $\lambda_3$ ,  $R_2$  and  $R_3$  denote two kinds of the degree of the coherence and those of the interaction regions for 2-jet and 3-jet, respectively. The values of  $R_2 = 0.83 \pm 0.05$  fm and  $R_3 = 1.09 \pm 0.04$  fm in Table 2 could be examined.

*Acknowledgments.* One of the authors (M.B.) would like to thank the colleagues of the Center for General Education at Shinshu University.

## A Analysis of L3 BEC by Eq. (2) with the adjustable parameter $R_a$

Table 9 presents our results by Eq. (2) with the adjustable parameter  $R_a$ . For free parameter  $R_a$ 's, we compare figures with the following exact parameter:  $R_a(2\text{-jet}) = 0.522$  fm and  $R_a(3\text{-jet}) = 0.613$  fm. Obviously there are differences between them. On the other hand, the effect of  $\text{LRC}_{(\text{linear})}$  is very small in Table 9. Anyhow, values of  $\chi^2/\text{dof}$  become smaller than those in Table 1. However, as  $R_a$ 's are free, the exactness of the Levy canonical form is relaxed.

Table 9: Fit parameters of data on 2-jet and 3-jet events by Eq. (2).  $R_a$  is treated as a free parameter. In the upper column,  $\delta = 0$  are used.

event	$R$ (fm)	$R_a$ (fm)	$\lambda$	$C$	$\alpha_\tau$	$\delta$ ( $\text{GeV}^{-1}$ )	$\chi^2/\text{dof}$
2-jet	$0.80 \pm 0.04$	$0.71 \pm 0.01$	$0.64 \pm 0.03$	$0.991 \pm 0.003$	$0.79 \pm 0.01$	—	91.7/95
3-jet	$1.07 \pm 0.05$	$0.88 \pm 0.02$	$0.93 \pm 0.04$	$0.998 \pm 0.001$	$0.70 \pm 0.02$	—	84.2/95
2-jet	$0.79 \pm 0.04$	$0.69 \pm 0.04$	$0.63 \pm 0.03$	$0.988 \pm 0.005$	$0.81 \pm 0.04$	$(1.5 \pm 2.0) \times 10^{-3}$	91.2/94
3-jet	$1.07 \pm 0.05$	$0.87 \pm 0.04$	$0.93 \pm 0.05$	$0.997 \pm 0.005$	$0.71 \pm 0.02$	$(-0.3 \pm 1.7) \times 10^{-3}$	84.1/94

## B Data on $N_{\text{MC}}^{(2+:2-)} / N_{\text{MC}}^{(+-)}$ at $Z^0$ -pole by DELPHI Collaboration

DELPHI Collaboration reported the data on  $N_{\text{MC}}^{(2+:2-)} / N_{\text{MC}}^{(+-)}$  at  $Z^0$ -pole by making use of JETSET 7.2 with DELSIM [14–16]. The data are analyzed by  $\text{LRC}_{(\text{Gauss})}$  and  $\text{LRC}_{(\text{Exp})} = C/(1 + \alpha \exp(-\beta Q))$  in Fig. 5.  $\text{LRC}_{(\text{Gauss})}$  seems to be better than  $\text{LRC}_{(\text{Exp})}$ . Note that  $\text{LRC}_{(\text{Exp})} \cong \text{LRC}_{(\text{linear})}$ . About data in the interval  $0.4 < Q < 0.8$  GeV, because of resonance effect from  $K^0$  and  $\rho^0$ , we do not use them in the present analysis. See also Ref. [14].

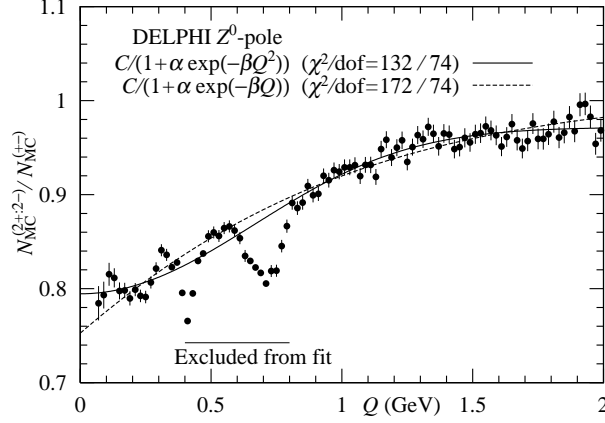


Figure 5: The single ratio on  $N_{\text{MC}}^{(2+;2-)} / N_{\text{MC}}^{(+;-)}$  by DELPHI Collaboration [14]. The parameters  $\alpha = 0.223 \pm 0.004$  and  $\beta = 1.42 \pm 0.06 \text{ GeV}^{-2}$  are estimated by  $\text{LRC}_{(\text{Gauss})}$ . For the black circle, their error bars are assumed 0.006 which are smaller than the smallest error bar (0.007).

## C Levy canonical form and formulation obtained by the inverse Fourier transformation ( $N = 1$ and $N = 4$ )

1) First, we show the proper time function  $H(\tau = \sqrt{t^2 - r_z^2})$  calculated by L3 Collaboration [1]. According to the notation in Ref. [1], the Levy canonical form with  $\zeta = \tan(\alpha_\tau \pi / 2)$  is expressed as

$$\tilde{H}(\omega) = \exp \left[ -\frac{1}{2}(\Delta r \omega)^\alpha (1 - i \text{sign}(\omega) \zeta) \right]. \quad (17)$$

The function  $H(\tau)$  is calculated by the inverse Fourier transformation as

$$\begin{aligned} H(\tau) &= \frac{1}{\pi} \int_0^\infty e^{-i\omega\tau} \tilde{H}(\omega) d\omega \\ &= \frac{1}{\pi} \text{Re} \left[ \int_0^\infty \exp \left( -\frac{1}{2}(\Delta r \omega)^\alpha - i\omega\tau + \frac{i}{2}(\Delta r \omega)^\alpha \zeta \right) d\omega \right] \\ &= \frac{1}{\pi} \int_0^\infty \exp \left( -\frac{1}{2}(\Delta r \omega)^\alpha \right) \cos \left( \omega\tau - \frac{1}{2}(\Delta r \omega)^\alpha \zeta \right) d\omega \\ &= H_{\text{cc}}(\tau) + H_{\text{ss}}(\tau) \end{aligned} \quad (18)$$

where cc and ss represent the products of  $\cos \cdot \cos$  and  $\sin \cdot \sin$  respectively. Using  $\Delta r = 1.56 \text{ fm}$  and  $\alpha = 0.47$ ,  $H(\tau)$ ,  $H_{\text{cc}}(\tau)$  and  $H_{\text{ss}}(\tau)$  are calculated (Fig. 6). The magnitudes of area presented in Fig. 6 are  $S \approx 0.9$  and  $S_{\text{cc}} = S_{\text{ss}} \approx 0.45$  in the range of  $0 \sim 50 \text{ fm}$ .

Combining the transverse and the rapidity distributions  $\rho(p_T)$  and  $\rho(y)$ , L3 Collaboration calculated their emitting source functions.

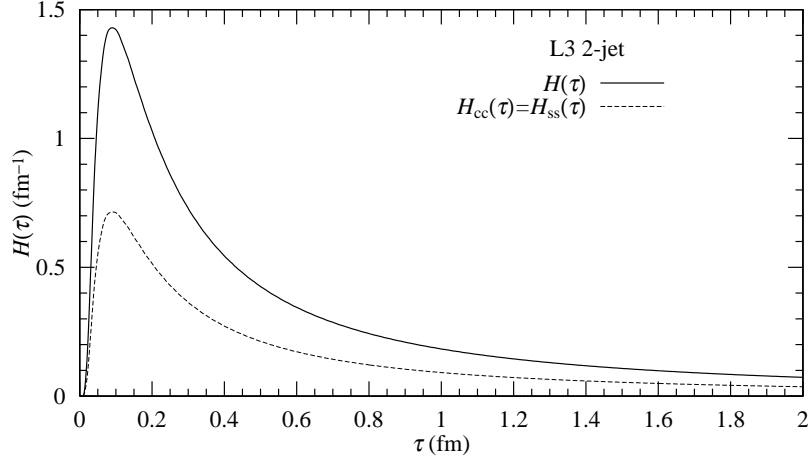


Figure 6: The probability  $H(\tau)$  of the Levy canonical form  $\tilde{H}(\omega)$  introduced by L3 Collaboration.

2) Second, to analyze the 2-jet events, they introduced the transverse mass  $a = 1/m_t$ . With the following identification,  $\Delta ra/2 = R^2$ , they started with the following Levy canonical form ( $N = 1$ ):

$$\tilde{H}_1(\omega) = \exp \left[ -\frac{1}{2}(R\omega)^{2\alpha}(1 - i \text{sign}(\omega)\zeta) \right]. \quad (19)$$

By making use the inverse Fourier transformation, the probability ( $N = 1$ )  $H_1(\xi_{12} = |x_1 - x_2|)$  is calculated as

$$H_1(\xi_{12} = |x_1 - x_2|) = \frac{1}{\pi} \int_0^\infty \exp \left[ -\frac{1}{2}(R\omega)^{2\alpha} \right] \cos \left[ \xi\omega - \frac{1}{2}(R\omega)^{2\alpha}\zeta \right] d\omega, \quad (20)$$

The results ( $R = 0.78$  fm,  $\alpha = 0.47$ ) are shown in Fig. 7. Two figures in Fig. 6 and Fig. 7 are different each other, because of difference between  $(\Delta r\omega)^\alpha$  and  $(R\omega)^{2\alpha}$ .

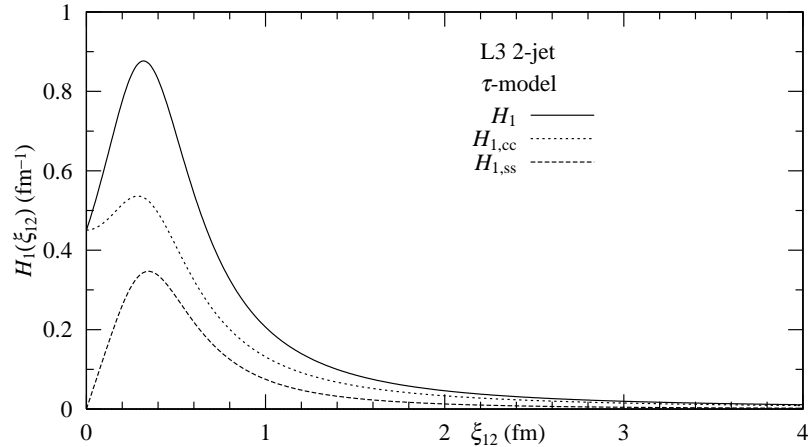


Figure 7: The probability  $H_1(\xi)$  of  $\tilde{H}_1(\omega)$ .

The magnitude of  $H(\xi_{12})$ ,  $S_1 = \int_0^\infty H(\xi_{12})d\xi_{12} \cong 0.75$  is computed in the range  $0 \sim 40$  fm. Because its magnitude, the name of probability for  $H(\xi_{12})$  seems to be unsuitable.

3) Third, L3 Collaboration adopted the following effective Levy form ( $N = 4$ ),

$$\tilde{H}_4(R\omega \rightarrow RQ) = \exp \left[ -\frac{1}{2}(RQ)^{2\alpha}(1 - i \text{sign}(Q)\zeta) \right]. \quad (21)$$

From Eq. (21), we calculate the probability  $P_\tau(\xi)$  as

$$\begin{cases} H_4(\xi) = \frac{1}{(2\pi)^2 \xi} \int_0^\infty Q^2 \exp\left(-\frac{1}{2}(RQ)^{2\alpha}\right) \cos\left(\frac{1}{2}(RQ)^{2\alpha}\zeta\right) J_1(Q\xi) dQ, \\ P_\tau(\xi) = 2\pi^2 \xi^3 H_4(\xi), \end{cases} \quad (22)$$

where  $\int_0^\pi \sin(\xi Q \cos \phi) \sin^2 \phi d\phi = 0$  is used.

The probability  $P_\tau(\xi)$  ( $R = 0.78$  fm,  $\alpha = 0.47$ ) is shown in Fig. 8. That the magnitude of  $S = \int P_\tau(\xi) d\xi \cong 1.0$  is computed. However, it is very strange that  $P_\tau(\xi)$  shows the partially negative behavior in the range of  $0 \sim 0.4$  fm:  $S_p \cong 1.04$  and  $S_n \cong -0.04$ , which mean the positive and the negative magnitudes, respectively [17, 18].

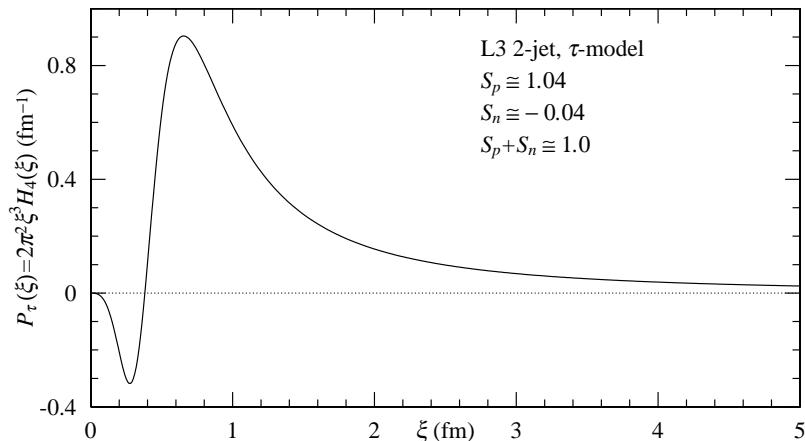


Figure 8: The probability  $P_\tau(\xi)$  calculated by Eq. (22).

The exchange function  $E_{\text{BE}}$  in the  $\tau$ -model is calculated as follows,

$$\begin{aligned} E_{\text{BE}} &= \text{Re} \left[ \tilde{H}_4^2(RQ) \right] \\ &= \exp\left(- (RQ)^{2\alpha}\right) \cos\left((RQ)^{2\alpha}\zeta\right). \end{aligned} \quad (23)$$

Introducing the degree of coherence  $\lambda$  and  $\text{LRC}_{(\text{linear})}$ , we obtain Eq. (2).

The stochastic density of exchange function  $E_{\text{BE}}$  in the  $\tau$ -model is calculated by the inverse Fourier transformation ( $N = 4$ ) as

$$\begin{cases} \rho_{\tau, \text{BE}}(\xi) = \frac{1}{(2\pi)^2 \xi} \int_0^\infty Q^2 \exp\left(- (RQ)^{2\alpha}\right) \cos\left((RQ)^{2\alpha}\zeta\right) J_1(Q\xi) dQ, \\ S_{\tau, \text{BE}}(\xi) = 2\pi^2 \xi^3 \rho_{\tau, \text{BE}}(\xi). \end{cases} \quad (24)$$

The profile of source function  $S_{\tau, \text{BE}}(\xi)$  in the  $\tau$ -model is described by a product of the phase  $2\pi^2 \xi^3$  and  $\rho_{\tau, \text{BE}}(\xi)$ . The source function  $S_{\tau, \text{BE}}(\xi)$  (with  $R = 0.78$  fm and  $\alpha = 0.47$ ) is shown in Fig. 9. We observe the partially negative behavior in the range  $0 < \xi < 0.6$  fm because of  $\cos((RQ)^{2\alpha}\zeta)$ .

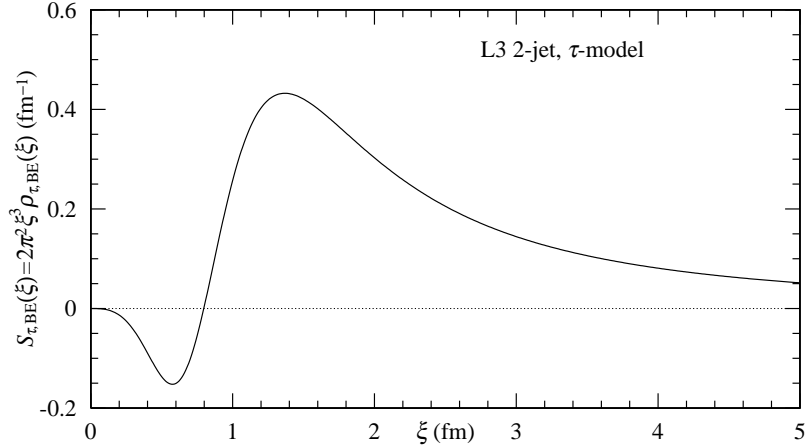


Figure 9: The profile of source function  $S_{\tau, BE}(\xi)$  in the  $\tau$ -model.

It should be distinguished that the probability  $P_\tau(\xi)$  and the source function  $S_{\tau, BE}(\xi)$ .

## References

- [1] P. Achard *et al.* [L3], *Eur. Phys. J. C* **71** (2011), 1648.
- [2] T. Mizoguchi, S. Matsumoto and M. Biyajima, *Int. J. Mod. Phys. A* **37** (2022) 25, 2250148.
- [3] T. Mizoguchi, S. Matsumoto and M. Biyajima, *Phys. Rev. D* **108** (2023) 5, 056014.
- [4] A. M. Sirunyan *et al.* [CMS], *JHEP* **03** (2020), 014.
- [5] V. Khachatryan *et al.* [CMS], *JHEP* **05** (2011), 029.
- [6] R. Shimoda, M. Biyajima and N. Suzuki, *Prog. Theor. Phys.* **89** (1993), 697-708.
- [7] M. Biyajima, *Phys. Lett. B* **92** (1980), 193.
- [8] M. Biyajima, A. Bartl, T. Mizoguchi, O. Terazawa and N. Suzuki, *Prog. Theor. Phys.* **84** (1990), 931-940.
- [9] R. Hanbury Brown and R. Q. Twiss, *Nature* **178** (1956), 1046-1048.
- [10] G. Goldhaber, S. Goldhaber, W. Y. Lee and A. Pais, *Phys. Rev.* **120** (1960), 300-312
- [11] V. V. Uchaikin, and V. M. Zolotarev, “Chance and stability: Stable distributions and their applications,” VSP, Utrecht, Netherlands, 1999.
- [12] F. Oberhettinger, “Tables of Fourier Transforms and Fourier Transforms of Distributions,” Springer, Berlin/Heidelberg, 1990.
- [13] I. S. Gradshteyn and I. M. Ryzhik, “Table of Integrals, Series, and Products,” 8th edition, Academic Press, Waltham, 2014.
- [14] P. Abreu *et al.* [DELPHI], *Phys. Lett. B* **286** (1992), 201-210.
- [15] T. Sjostrand and M. Bengtsson, *Comput. Phys. Commun.* **43** (1987), 367.
- [16] 16 DELPHI Collaboration, “Comparison of data with QCD models,” contributed paper to the LP-EPS conference, Geneva, August 1991.

- [17] J. P. Nolan, "Univariate Stable Distributions: Models for Heavy Tailed Data," Springer Nature, Switzerland, 2020.
- [18] V. M. Zolotarev, "One-dimensional stable distributions," Translations of Mathematical Monographs Vol. 65, American Mathematical Society, Providence, 1986.